IEEE Access
Multidisciplinary | Rapid Review | Open Access Journal

SPECIAL SECTION ON UNDERWATER WIRELESS COMMUNICATIONS AND NETWORKING

Received December 6, 2017, accepted January 15, 2018, date of publication January 23, 2018, date of current version April 18, 2018.

Digital Object Identifier 10.1109/ACCESS.2018.2795600

Mobile Node Localization in Underwater Wireless Networks

CUIE ZHENG[1,2], (Member, IEEE), DAJUN SUN[1,2], (Member, IEEE), LIN CAI[3], (Senior Member, IEEE), AND XIANG LI[1,2]

[1]College of Underwater Acoustic Engineering, Harbin Engineering University, Harbin 150001, China
[2]Science and Technology on Underwater Acoustic Laboratory, Harbin Engineering University, Harbin 150001, China
[3]Department of Electrical and Computer Engineering, University of Victoria, Victoria, BC V8W 3P6, Canada

Corresponding author: Cuie Zheng (zhengcuie@hrbeu.edu.cn)

This work was supported in part by the National Natural Science Foundation of China under Grant 61531012 and Grant 61701132, in part by the Heilongjiang Overseas Returnees Merit Funding under Grant 2017QD0047, in part by the Natural Sciences and Engineering Research Council of Canada, and in part by the Chinese Scholarship Council.

ABSTRACT Localizing mobile nodes in underwater networks is a highly challenging endeavor due to range errors caused by the mobility and uncertainty of sound speed. We propose a novel localization approach, which incorporates time alignment and range bending compensation to meet this challenge. Given the lengthy and varied propagation delays to different anchor nodes, we use a Kalman filter to align different time instants and locations as a mobile node receives timestamps from different anchors during a localization period. Based on Snell's law, the ray tracing theory is applied to compensate for sound speed variations. These two steps minimize the errors caused by mobility and sound speed uncertainty. A penalty convex–concave procedure approach is also applied to accurately solve a nonconvex optimization problem to minimize localization errors. Deep sea trial results show that the final localization error for the mobile node is only 1.44 m (with the differential GPS as the true-value reference), marking a substantial improvement over existing state-of-the-art solutions.

INDEX TERMS Underwater network localization, mobile node, time alignment, ray tracing.

I. INTRODUCTION

Underwater wireless sensor networks (UWSN) with mobile nodes have garnered a great deal of research interest given their many potential applications in the marine science and technology field [1]. Various types of underwater unmanned vehicles (UUVs), such as AUVs and gliders, may serve as UWSN mobile nodes [2]. They can be equipped with acoustic modems and detection sensors such as multi-beam sonar, biosensors, or chemical sensors for various tasks. Accurate localization of these devices is essential to ensure the accuracy of the data they gather.

As opposed to terrestrial WSNs, global positioning system (GPS) signals fade rapidly in water and are not suitable for UWSN localization [3]. The received signal strength indicator (RSSI) ranging method widely applied to terrestrial WSN localization is also ill-suited to UWSNs due to the complexity of the underwater acoustic channel and the high cost of pre-sampling on-site [4]. UWSN localization often relies on measuring the distances between nodes using the time difference of arrival (TDoA) or time of arrival (ToA). A target node can be localized by triangulation or trilateration after measuring the distances to anchor nodes repeatedly.

Distance measurement for mobile nodes in UWSNs is essential [5], but is hindered by three main challenges:

First, as opposed to the constant RF signal propagation speed in air, sound speed in water varies with temperature, salinity, and water pressure forming highly nonlinear sound speed profiles [6]. Early research on UWSN localization was typically conducted under the assumption that acoustic signals propagate at a nominal speed of 1500 m/s, which may introduce severe estimation errors [7]. The average sound speed may instead be treated as an unknown parameter to be solved together with the locations [8]. This approach assumes a constant average acoustic velocities for all nodes in the network. For UWSNs with different depths or different horizontal distances, however, the acoustic velocity between a pair of nodes may deviate from the average speed.

Second, unlike the terrestrial WSNs in which the signal propagates along a straight line, acoustic rays bend in

UWSNs; this may also introduce severe range estimation error if not appropriately addressed [7].

Third, during a message exchange period, a mobile node may move to different locations when receiving signals from different anchors. For low-speed mobile nodes such as drifting targets, a time window can be used to bound such movement and avoid significant errors [8]. For mobile nodes such as AUVs, it is very difficult to achieve both precision and efficiency in localization due to the speed of their movement. Yi *et al.* [9], [10] proposed the use of mobile node inertial navigation for compensation, but not all mobile nodes can be equipped with accurate inertial navigation.

Previous researchers have addressed the above challenges with a joint solution for localization and synchronization (JSL) [11]. JSL performs tracking compensation for the sound ray curve using the Fermat's principle for UWSN localization, and an interactive multiple model (IMM) filter to reduce the localization error caused by the mobility. JSL can handle sporadical location outliers; when a burst of outliers appear, the IMM filter diverges. The inherent multipath characteristics of underwater acoustic channels may introduce bursty range estimation outliers, which cannot be handled well by JSL. Thus, how to accurately localize mobile nodes in UWSN remains an open and challenging problem.

In this study, we addressed the above three challenges using the time alignment (TA) and ray tracing (RT) techniques to achieve a localization accuracy for mobile nodes in UWSNs. Given the transmission time delay between the mobile node and anchor nodes in a UWSN, we first attempt to eliminate the model error caused by the different locations of mobile node as they receive the timestamps from different neighboring anchor nodes within one localization period. Based on timestamps exchanged between the mobile and anchor nodes, the proposed localization algorithm uses a Kalman filter to align the distances between different neighboring nodes and the mobile node for accurate time delay estimation. We also attempt to correct the range estimation error caused by ray bending. We apply a ray tracing technique based on Snell's law to remove the ray bending error and to renew the Kalman filter, then run a special initialization method to initialize and feedback the Kalman filter. We then formulate the localization problem with unknown varying sound speed as a nonconvex localization optimization problem which can be solved via the penalty convex-concave procedure (PCCP). We conducted a shallow water test in Qiandao Lake and a deep sea trial in the South China Sea to find that the final mobile node root-mean-square (RMS) localization error of our algorithm is only 1.44 m (with differential GPS as the true-value reference). Throughout these tests, the proposed approach outperformed other state-of-the-art methods under real-world conditions.

The rest of this paper is organized as follows. The system model is presented in Section II. In Section III, we describe the proposed localization algorithm including its general architecture and detailed implementation. Field test results (both shallow water and deep sea) are presented in Section V, followed by concluding remarks and a discussion on future research directions in Section VI.

II. SYSTEM MODEL

Consider a synchronized UWSN with N_a anchor nodes which have known locations, as well as mobile nodes with unknown locations in a three-dimensional underwater space. No three anchor nodes are collinear. Without loss of generality, we focus on localizing only one mobile node in a given time period. Denote $\boldsymbol{u}_i = \begin{bmatrix} u_{xi} & u_{yi} & u_{zi} \end{bmatrix}, i \in \{1, 2, \cdots N_a\}$ as the position of the i-th anchor node, and $\boldsymbol{v} = \begin{bmatrix} v_x & v_y & v_z \end{bmatrix}$ as the position of the mobile node. Assume that the mobile node is equipped with a pressure sensor, so v_z can be obtained from the pressure reading. The goal of this work is to estimate v_x and v_y.

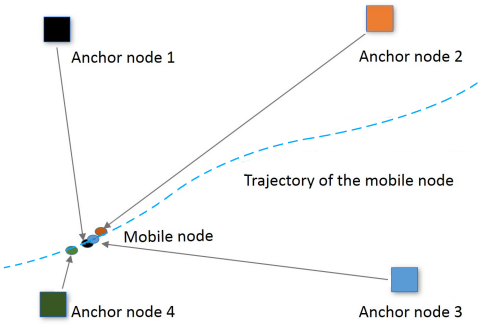

FIGURE 1. Localization scenario.

As shown in Fig. 1, we rely on one-way packet broadcasting from the neighboring anchor nodes to the mobile node. Assume that there are L messages being sent from the neighboring anchor node A_i to the mobile node B during the localization procedure.

For the k-th packet transmission, anchor node A_i broadcasts its localization message at time T_{ik}. Node B receives this localization message at time R_{ik} and obtains v_{zk} at R_{ik} from the pressure sensor. Therefore, after the k-th message is broadcasting, node B has obtained the localization information $\{T_{ik}, R_{ik}, u_{xi}, u_{yi}, u_{zi}, v_{zk}\}$. The measured transmission time and distance for the k-th message from the neighboring anchor node A_i to node B can then be calculated as follows.

$$t_{ik} = R_{ik} - T_{ik}, \tag{1}$$

and

$$r_{ik} = f\left(C\left(z\right), t_{ik}\right), \tag{2}$$

where $C(z)$ is the acoustic velocity, which is a function of the depth. Using a realistic function, $C(z)$, instead of a constant velocity can help to improve the localization accuracy.

The distance between the mobile node and its neighboring anchor node can also be expressed as the norm of the coordinate difference between two nodes based on the geometric relationship:

$$r_{ik} = \|\boldsymbol{v}_k - \boldsymbol{u}_i\|, \quad k = 1, 2, \ldots, N_a. \tag{3}$$

The localization problem can be modeled as the following optimization problem.

$$\boldsymbol{v}_k = \arg\min_{\boldsymbol{v}_k \in \mathbb{R}^3} \sum_{i=1}^{N_a} (f(C(z), t_{ik}) - \|\boldsymbol{v}_k - \boldsymbol{u}_i\|)^2 \quad (4)$$

We attempt to localize the mobile node by solving Eq. (4) using the anchor locations, timestamp information, depth sensor information, and acoustic velocity profile.

III. LOCALIZATION ALGORITHM

A. OVERVIEW

In this section, we propose a novel localization algorithm for UWSN mobile nodes, called "TA-PCCP-RT". "TA" represents time alignment; a Kalman filter is used to align the different time instants at which the mobile node receives messages from different anchor nodes. "PCCP" represents the penalty convex-concave procedure, which is used to solve the localization optimization problem. "RT" represents the ray tracing technique based on Snell's law, which is used to remove the ray bending error.

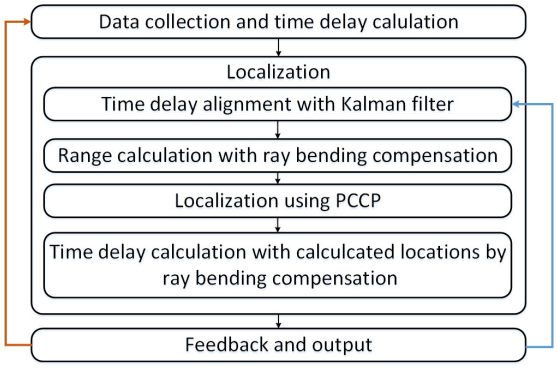

FIGURE 2. Flow chart of TA-PCCP-RC.

The TA-PCCP-RT localization algorithm works in three stages, as shown in Fig. 2. The first stage involves data collection and time delay calculation using Eq. (1). In this stage, the anchor nodes broadcast their locations and transmit timestamps after receiving a localization request from the mobile mode. The mobile node stores the information of the anchor nodes and records the receiving time and its depth when receiving any message from a neighbouring anchor node. The location of the previous cycle is also calculated in the current message exchange cycle. Node localization is possible when messages from more than two neighboring anchor nodes have been collected properly. Generally speaking, localization accuracy can be improved substantially when messages from four or more neighboring anchor nodes have been collected properly. Here, "properly" means that the received messages have not suffered from multipath interference.

The second stage involves TA-aided localization. The distance between different anchor nodes and the mobile node are different. Even if the anchor nodes transmit at the same time, their respective messages will reach the mobile node at different time points. The mobile node moves across different locations when receiving these messages. Time alignment is necessary to use these messages to localize the mobile node in a given instant; the output of the first stage (TA) thus serves as the input in the second stage. There are three steps in this stage. First, the time delays are aligned by a Kalman filter; second, ray tracing is employed to compensate for sound ray refraction to obtain accurate distance information; and finally, PCCP is deployed for localization computation. We also calculate the time delay using the locations from the last step (ray tracing) for enhanced accuracy. This inversely calculated time delay can be used to correct the state of the Kalman filter and improve the accuracy of the subsequent prediction.

The last stage involves feedback and output. The steps of the second and third stages are described in detail below.

B. LOCALIZATION PROCEDURE

1) STEP1, TIME DELAY ALIGNMENT

As shown in Fig. 1, as opposed to localizing a static node in UWSNs, there is a model error caused by the different locations of the mobile node when it receives timestamps from different anchor nodes within one localization period. This error could be easily eliminated if the velocity of the mobile node is known. In reality, the mobile node may not be equipped with an INS. In this study, we were able to rely only on the locations of anchor nodes and the timestamps for receipt and transmission, so we used a Kalman filter to achieve time alignment. The Kalman filter can also eliminate severe time delay errors and filter out noise. The filter performs well if the object model is accurate and the statistics of parameters are relatively stable; it also works well in real-time and requires relatively little storage. Kalman filter performs well if the object model is accurate and the statistics of parameters are relatively stable, and it is simple to work in real time and requires a small storage only.

The Kalman filter works in a two-step process: the prediction step and the correction step [12]. In the first step, the filter produces estimates of the current state variables. In the second step, the filter uses the measurements to modify the prediction model.

The movement velocity of a buoy node, one of the most common types of mobile nodes in a UWN, is usually less than 1 m/s. Given maneuver-based movement, the speed of a mobile AUV nodes typically ranges from 1 to 4 m/s. We selected the Constant Acceleration (CA) model and directly established the basic equation for filtering accordingly [13].

Time is discretized. We use subscript k to refer to time instant t_k. We denote by $\mathbf{T}_k = \left[t_k, \dot{t}_k, \ddot{t}_k\right]$ the estimator at t_k, $\boldsymbol{\Phi}_{k,k-1}$ the state transition model from t_{k-1} to t_k, $\boldsymbol{\Gamma}_{k-1}$ the control-input model, w_{k-1} the time delay noise sequences, and $\mathbf{H}_k$ as the measurement model, respectively.

The iterative procedure of the Kalman filter is given as follows [13]. One-step state prediction is given by:

$$\hat{\mathbf{T}}_{k/k-1} = \mathbf{\Phi}_{k,k-1}\hat{\mathbf{T}}_{k-1}. \tag{5}$$

The mean square error of one-step prediction is calculated as follows:

$$\mathbf{P}_{k/k-1} = \mathbf{\Phi}_{k,k-1}\mathbf{P}_{k-1}\mathbf{\Phi}_{k,k-1}^T + \mathbf{\Gamma}_{k-1}\mathbf{Q}_{k-1}\mathbf{\Gamma}_{k-1}^T. \tag{6}$$

Filtering gain

$$\mathbf{K}_k = \mathbf{P}_{k/k-1}\mathbf{H}_k^T(\mathbf{H}_k\mathbf{P}_{k/k-1}\mathbf{H}_k^T + \mathbf{R}_k)^{-1}. \tag{7}$$

State estimation

$$\hat{\mathbf{T}}_k = \hat{\mathbf{T}}_{k/k-1} + \mathbf{K}_k(\mathbf{Z}_k - \mathbf{H}_k\hat{\mathbf{T}}_{k/k-1}). \tag{8}$$

The estimated mean square error can be derived as follows:

$$\mathbf{P}_k = (\mathbf{I} - \mathbf{K}_k\mathbf{H}_k)\mathbf{P}_{k/k-1}(\mathbf{I} - \mathbf{K}_k\mathbf{H}_k)^T + \mathbf{K}_k\mathbf{R}_k\mathbf{K}_k^T \tag{9}$$

where $\mathbf{H}_k = \begin{bmatrix}1 & 0 & 0\end{bmatrix}$, $\mathbf{\Phi}_{k,k-1} = \begin{bmatrix}1 & T & T^2/2\\ 0 & 1 & T\\ 0 & 0 & 1\end{bmatrix}$, and $\mathbf{\Gamma}_{k-1} = \begin{bmatrix}T^3/6 & T^2/2 & T\end{bmatrix}^T$.

The state equation for time delay filtering is

$$\mathbf{T}_k = \mathbf{\Phi}_{k,k-1}\mathbf{T}_{k-1} + \mathbf{\Gamma}_{k-1}w_{k-1}, \tag{10}$$

where w_{k-1} are the time delay noise sequence.

The measurement for time delay filtering is

$$z_k = \mathbf{H}_k\mathbf{T}_k + v_k, \tag{11}$$

where z_k is the measured value of the time delay from the target to the transponder, and v_k is the sequence of the time delay measurement noise. Time delay can be accurately normalized to the same sampling time to compensate for the localization error introduced by target movement using Eq. (10).

Setting the initial values is an important issue in Kalman filter design. This may result in significant initial localization errors or outliers in UWSN, however, given the complicated underwater acoustic channels and node mobility. Although a certain level of fault tolerance is allowed by the Kalman filter as the filter converges gradually after a period of time, any error in the initial value negatively impacts the initial filtering effect. A larger error indicates poor initial filtering effect and less accurate estimated value [14].

Another approach is to obtain the time delay data within a specific duration before applying the Kalman filter [15]. This involves assigning the average value of the time delays of various branches to t0, then using time delay data in this period to estimate the matrix of the initial covariance P0. This requires information exchange over a very long time period for initial value selection, making the cost too high for any UWN with a low data transmission rate and long propagation delay.

As a departure from the literature, in this work, we determine the initial filtering value by judging the quality of time delay measurements. Considering the sparse characteristics of the UWSN, it is difficult to find a node surrounded by many anchor nodes. In the references involving real UWSN tests [8], [10], [16], [17], the number of the neighboring anchor nodes is typically between four and five while the distance and propagation delay between nodes varies substantially, unlike land WSNs. The four anchor nodes with the closest timestamps are always selected for localization, which reduces the difference in received signals arising from distance variations when the information packets from multiple anchor nodes are received.

The anchor nodes are divided into two sets, $\mathcal{N}_{a1}$ and $\mathcal{N}_{a2}$, during the initial filtering value selection procedure. Set $\mathcal{N}_{a1}$ contains the four anchor nodes with the closest time delay as detected by the mobile node to be localized; $\mathcal{N}_{a2}$ is the set containing remaining anchor nodes.

The time delay filter of the anchor nodes in $\mathcal{N}_{a1}$ is recorded as t_{jk} $(j = 1, 2, 3, 4)$. The range of $\mathcal{N}_{a1}$ can be calculated using the constant sound speed:

$$r_{jk} = Ct_{jk} \quad (j = 1, 2, 3, 4)\,. \tag{12}$$

Three different locations of the node, $\boldsymbol{v}_{kj}$ $(j = 1, 2, 3)$, can be preliminarily determined by Eq. (4) with three different combinations from $\mathcal{N}_{a1}$. The standard deviation of these three locations σ_k can be calculated accordingly.

If there are two neighboring σ_k no larger than a preset threshold DT_p, the time delay calculated from the timestamps directly serves as the initial value of the time delay filter for anchor nodes in $\mathcal{N}_{a1}$:

$$\mathbf{T}_{jk} = \left[t_{jk}, {}^{(t_{jk} - t_{j(k-1)})}\!/_{T}, 0\right], \tag{13}$$

$$P_k = {}^{1}\!/_{3}\sum_{j=1}^{4}\left(t_{jk} - t_{k0}\right)^2, \tag{14}$$

$$t_{k0} = {}^{1}\!/_{4}\sum_{j=1}^{4} t_{kj}, \quad j = 1, 2, 3, 4. \tag{15}$$

The target node location, v_k, can simultaneously be calculated by according to the time delay of $\mathcal{N}_{a1}$ by ray tracing.

The locations, $\boldsymbol{v}_k$ and $\boldsymbol{v}_{k-1}$, can then be calculated by the ray tracing techniques with the SVP, time delay and coordinates from $\mathcal{N}_{a1}$. Then, $\widetilde{t}_{mk}, \widetilde{t}_{m(k-1)}$, the propagation time delay from the mobile node to the anchor nodes in $\mathcal{N}_{a2}$, is recalculated by ray tracing techniques with $\boldsymbol{v}_k, \boldsymbol{v}_{k-1}$, using the anchor nodes coordinates and SVP. This time delay serves as the initial time delay filtering value corresponding to the anchor nodes in $\mathcal{N}_{a2}$:

$$\mathbf{T}_{mk} = \left[\widetilde{t}_{mk}, {}^{(\widetilde{t}_{mk} - \widetilde{t}_{m(k-1)})}\!/_{T}, 0\right]. \tag{16}$$

This specific Kalman filter initial value selection Algorithm 1 is deployed for anchor nodes newly detected in the subsequent localization procedure. The initial time delay filer value is determined in the same manner as anchor nodes in $\mathcal{N}_{a2}$.

Algorithm 1 Kalman Filter Initialization

Input: time delay, average sound velocity C, sound speed profile $C(z)$, coordinate of anchor nodes, position error threshold DT_p
Output: $\mathbf{T}_{ik}$, P_k
Flag = true;
while *Flag* **do**
  if $N_{anchor} < 4$ **then**
    $Counter = 0$; continue;
  end
  else
    Select the 4 anchor nodes with the closest time delay to constitute $\mathcal{N}_{a1}$, and the rest anchor nodes constitute $\mathcal{N}_{a2}$;
    Calculate the range r_{jk} by (12);
    Solve $\boldsymbol{v}_{kj}$ by (4);
    Calculate σ_k;
    if $\sigma_k \leq DT_p$ **then**
      $Counter = Counter + 1$;
    end
    else
      $Counter = 0$;
    end
    if $Counter = 2$ **then**
      For set $\mathcal{N}_{a1}$, set the initial value $\mathbf{T}_{jk}$, P_k, t_{k0} as (13)-(15);
      Calculate the location $\boldsymbol{v}_k$, $\boldsymbol{v}_{k-1}$ by information from $\mathcal{N}_{a1}$;
      For set $\mathcal{N}_{a2}$, re-calculate the time delay $\widetilde{t}_{mk}$, $\widetilde{t}_{m(k-1)}$;
      set the initial value $\mathbf{T}_{mk}$ as (16);
      Flag = false;
      Break;
    end
  end
end
return $\mathbf{T}_{ik}$, P_k;

2) STEP 2, RANGE CALCULATION WITH RAY TRACING

Denote the sound velocity vertical section function as $C(z)$, where z is the depth with the acoustic source as the reference point. The function of the grazing angle changing with depth is $a\,(z|\alpha_0)$, where α_0 is the initial grazing angle of the sound ray starting from the transmitter.

Denote the depths of the transmitting node and receiving node by z_0 and z_1, respectively. The horizontal distance between the acoustic source to the target is:

$$x = \int_{z_0}^{z_1} \frac{dz}{\tan\left(\alpha\,(z|a_0)\right)} = \cos\alpha_0 \int_{z_0}^{z_1} \frac{dz}{\sqrt{(C_0/C\,(z))^2 - \cos^2\left(\alpha_0\right)}}. \tag{17}$$

If the depth of the working water area is Z, the sound velocity profile function of the area is $C(z)$. As shown in Fig. 3,

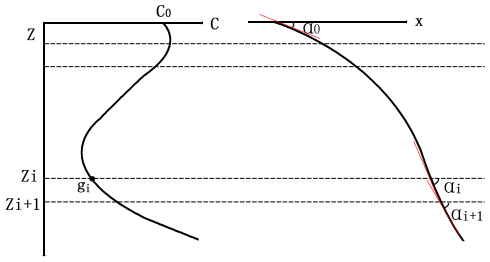

FIGURE 3. Ray tracing algorithm.

the depth range is divided into N connected water layers comprised of $z_1, z_2, \ldots, z_N$. The acoustic ray is assumed to propagate in a constant gradient manner in each layer. The acoustic ray propagation between different layers follows the Snell's law,which can be expressed as follows:

$$\frac{\cos\alpha_l}{C_l} = \frac{\cos\alpha_0}{C_0} = p, \tag{18}$$

where α_l is the grazing angle, C_l is the acoustic velocity, and α_0 and C_0 are the values corresponding to outgoing sound ray location.

If the initial grazing angle α_0 and the vertical layering distribution of the acoustic velocity $C(z)$ are known, the grazing angle of the sound ray at any depth can be obtained according to the Snell's law, and thus the acoustic wave's propagation direction at any depth can be obtained. Different α can be obtained from different initial grazing angles; these values correspond to different sound ray traces.

Assume that the $(l+1)$th layer is located between depth z_l and z_{l+1}, with grazing angle distribution of α_l and α_{l+1}, and horizontal propagation distance of x_{l+1}. The sound ray is a circular arc with a curvature of F_l, and the gradient is approximately constant in each layer. The acoustic velocity gradient in layer l is defined as g_l:

$$g_l = \frac{C_{l+1} - C_l}{z_{l+1} - z_l}. \tag{19}$$

The curvature is given by

$$F_l = \frac{-1}{pg_l}. \tag{20}$$

The horizontal propagation distance and propagation time delay in each layer are, respectively,

$$x_l = F_l\left(\sin\alpha_l - \sin\alpha_{l-1}\right) = \left|\frac{C_0}{\cos\alpha_0 g_l}\left(\sin\alpha_l - \sin\alpha_{l-1}\right)\right|, \tag{21}$$

and

$$t_l = \frac{(\alpha_{l-1} - \alpha_l)}{pg_l^2 \Delta z_l} \ln\left(\frac{C_l}{C_{l-1}}\right). \tag{22}$$

The final horizontal range and propagation time delay of the acoustic transmitting path are

$$x = \sum x_l, \tag{23}$$

and

$$t = \sum t_l. \tag{24}$$

Once the propagation time and SVP are known, the bisection method can be applied to search the grazing angle and accurately calculate the distance of the acoustic transmitting path.

3) STEP 3, LOCALIZATION USING PCCP

It is difficult to obtain the global optimal solution directly because the localization objective function of Eq. (4) is nonconvex,so we focus on obtaining an approximate solution. In 2004, Cheung *et al.* [18] proposed a semidefinite relaxation method to obtain an accurate approximate global solution. In 2008, in response to a series of issues regarding the least-square solution proposed in 2004, Beck [19] converted the SR least-square structure into generalized trust region subproblems to solve the basic localization equation. In 2016, Darya and Wu-Sheng [20] discovered that such problems can be solved by the PCCP approach. Localization accuracy can be improved significantly by PCCP compared to SR least-square. A full convergence analysis of PCCP can be found in our references [21].

We apply the PCCP method here to solve the localization problem. PCCP combines convex optimization and local optimization by converting a nonconvex optimization problem into an approximate optimization problem. The solution for the approximate convex optimization serves as the initial value of the local optimization algorithm for solving the original nonconvex problem.

The objective function $F(\boldsymbol{v}_k)$ in Eq. (4) can be expressed as follows

$$\begin{aligned} F(\boldsymbol{v}_k) &= N_a {\boldsymbol{v}_k}^T \boldsymbol{v}_k - 2{\boldsymbol{v}_k}^T \sum_{i=1}^{N_a} \boldsymbol{u}_{ik} \\ &\quad - 2\sum_{i=1}^{N_a} f(C(z), t_{ik}) \left\| \boldsymbol{v}_k - \boldsymbol{u}_{ik} \right\| \\ &= f(\boldsymbol{v}_k) - g(\boldsymbol{v}_k), \end{aligned} \tag{25}$$

where

$$f(\boldsymbol{v}_k) = N_a {\boldsymbol{v}_k}^T \boldsymbol{v}_k - 2{\boldsymbol{v}_k}^T \sum_{i=1}^{N_a} \boldsymbol{u}_{ik}, \tag{26}$$

and

$$g(\boldsymbol{v}_k) = 2\sum_{i=1}^{N_a} f(C(z), t_{ik}) \left\| \boldsymbol{v}_k - \boldsymbol{u}_{ik} \right\|. \tag{27}$$

where $f(\boldsymbol{v}_k)$ and $g(\boldsymbol{v}_k)$ are convex functions. The localization problem in Eq. (4) is expressed as a target function of a standard difference of convex (DC) form $F(\boldsymbol{x}) = f(\boldsymbol{x}) - g(\boldsymbol{x})$. The PCCP method can be used to solve such problems via affine approximation $g(\boldsymbol{x})$ at the initial value $\boldsymbol{x}^{(q)}$:

$$\hat{g}(\boldsymbol{x}, \boldsymbol{x}^{(q)}) = g(\boldsymbol{x}^{(q)}) + \nabla g(\boldsymbol{x}^{(q)})^T (\boldsymbol{x} - \boldsymbol{x}^{(q)}). \tag{28}$$

$F(\boldsymbol{x}) = f(\boldsymbol{x}) - g(\boldsymbol{x})$ becomes a convex function, then affine approximation is performed for the constraint conditions. The DC structural optimization problem is approximated as a convex optimization problem for obtaining the local minimum $\boldsymbol{x}^{(q+1)}$. Circulative iteration is performed for $\boldsymbol{x}^{(q)} = \boldsymbol{x}^{(q+1)}$ until the target function falls below the threshold.

The error bound of the range estimation, which depends on the time delay estimation error and the sound speed error, is δ_{ik}. The constraints are:

$$\begin{cases} \|\boldsymbol{v}_k - \boldsymbol{u}_{ik}\| \le f(C(z), t_{ik}) + \delta_{ik}, \\ f(C(z), t_{ik}) - \delta_{ik} \le \|\boldsymbol{v}_k - \boldsymbol{u}_{ik}\|. \end{cases} \tag{29}$$

After the affine approximation for both the objective function $g(x)$ and the constraints, and adding the constraint variable and penalty function, the localization problem can be formulated as a PCCP problem:

$$\begin{aligned} \min_{\boldsymbol{v}_k, h_{ik}, \hat{h}_{ik}} \quad & {\boldsymbol{v}_k}^T \boldsymbol{v}_k - 2{\boldsymbol{v}_k}^T \Big(\frac{1}{N_a}\sum_{i=1}^{N_a} \boldsymbol{u}_{ik} \\ & + \frac{1}{N_a}\sum_{i=1}^{N_a} f(C(z), \partial \left\| {\boldsymbol{v}_k}^{(l)} - \boldsymbol{u}_{ik} \right\|) \\ & + {g_k}^{(q)} \sum_{i=1}^{N_a} (h_{ik} + \hat{h}_{ik}) \\ s.t.: \quad & \left\| {\boldsymbol{v}_k}^{(q)} - \boldsymbol{u}_{ik} \right\| - f(C(z), t_{ik}) - \delta_{ik} \le h_{ik}, \\ & - \left\| {\boldsymbol{v}_k}^{(q)} - \boldsymbol{u}_{ik} \right\| - \partial \left\| {\boldsymbol{v}_k}^{(q)} - \boldsymbol{u}_{ik} \right\|^T ({\boldsymbol{v}_k} - {\boldsymbol{v}_k}^{(q)}) \\ & + f(C(z), t_{ik}) - \delta_{ik} \le \hat{h}_{ik}, \\ & h_{ik} \ge 0, \hat{h}_{ik} \ge 0, \ \forall i = 1, 2, \ldots, N_a. \end{aligned} \tag{30}$$

Algorithm 2 yields the solution to the PCCP problem.

4) STEP 4, INVERSE COMPUTATION OF TIME DELAY

The inverse time delay computation uses the relatively accurate mobile node location obtained in Step 3 and the inverse ray-tracing time delay solution to correct the state of the Kalman filter, which further enhances the accuracy of the subsequent prediction. The bisection method and Snell's law are applicable when the positions of the mobile node and anchor nodes are known. The time delay obtained from Eq. (24) is the propagation time delay of the inverse sound ray tracing solution when the horizontal distance obtained from Eq. (23) is equal to the horizontal distance obtained from the actual coordinates.

C. FEEDBACK AND OUTPUT

In addition to the direct path signal, the underwater acoustic channel (UWAC) consists of groups of non-direct paths [22]. The multipath environment comprises large time delay and small time delay paths. If the delay difference from the direct path is below the system resolution, the paths are small time delay paths; otherwise, they are large time delay paths. Large time delay paths typically do not influence the processing

Algorithm 2 PCCP Localization

Input: Node location $\boldsymbol{u}_{ik}$, time delays t_{ik}, sound velocity profile $C(z)$, initial value of location $\boldsymbol{v}_k{}^{(0)}$, maximum number of iterations $l_{\max}$, initial penalty factor $g_k{}^{(0)}$, maximum penalty factor $g_{k\max}$, growth coefficient of penalty factor μ, constraint boundary δ_{ik}, threshold DT_{pccp}

Output: $\boldsymbol{v}_k$

while *Flag* **do**

  Calculate the range $r_{ik} = \int_z \frac{dz}{\tan(\alpha(z|a_0))}$ by ray tracing using t_{ik} and sound velocity profile $C(z)$;

  if $q \le q_{\max}$ **then**

    Establish a convex optimization function by using (30);

    Obtain the variable $\boldsymbol{v}_k{}^{(q)}$, $h_{ik}{}^{(q)}$, $\hat{h}_{ik}^{(q)}$;

    Update the penalty factor;

    Update the location $\boldsymbol{v}_k = \boldsymbol{v}_k{}^{(q)}$;

    if $q \ge 1$ *and* $\left\|\boldsymbol{v}_k{}^{(q)} - \boldsymbol{v}_k{}^{(q-1)}\right\| \le DT_{pccp}$ **then**

      Break;

    end

    $q = q + 1$;

  end

end

Return $\boldsymbol{v}_k$;

of the direct path. The amplitude of the direct path signal commonly is not the highest among the multiple paths. The multipath characteristics cause estimation errors ranging from several ms to several hundreds of ms [23]. They can substantially degrade the overall ranging accuracy and thus the localization performance; they may additionally lead to Kalman filter divergence [24]. Large measurement errors in the filter also affect the subsequent data. In fact, errors in the filter output data may be more severe than those in the source data, particularly when the underwater acoustic channel is subjected to significant interference or sudden changes.

In this study, we designed a judgment method for feedback and output to replace the direct output feedback of the Kalman filter. It is a two-step process. First, the quality of the input data (time delays before the Kalman filter) and the filtering output data is judged. When the latest input data is of high quality while the preorder input data has poor quality, there are significant differences between the localization results by the time delays with and without the filter; the latest input data should be used and the current Kalman filter output should be discarded (i.e., the Kalman filter should be restarted). Data quality is judged in the same way as that data are selected when determining the initial filter parameters.

Second, the high-accuracy node position information is gathered and the ray tracing inverse solution time delay is substituted for the inverse computation time delay. As discussed above, this time delay value replaces the direct output of Kalman filter to feedback in order to correct the Kalman filter state and enhance the accuracy of the subsequent prediction.

We believe the TA-PCCP-RT localization algorithm can significantly improve the localization accuracy for UWSN mobile nodes. Our field test results validate its performance, as discussed below.

IV. BOUND DISCUSSION

This section discusses our derivation of the upper and lower bounds for the localization algorithm. The total error is consists of systematic error and random error. Systematic error in the estimator of $\boldsymbol{v_k}$ is caused by the ray bending and the time delay misalignment due to the node's mobility. The random error is mainly caused by the time delay estimation. Here, we denote ε_{rms} as the total error, σ_r as the random error, ε_t as the systematic error caused by the node mobility, and ε_c as the systematic error caused by the ray bending. We consider the upper bound of $\boldsymbol{v_k}$ to have both systematic error and random error.

$$\varepsilon_{rms}^2 = \sigma_r^2 + \varepsilon_t^2 + \varepsilon_c^2 \tag{31}$$

Equation (4) can be rewritten as follows:

$$r_{ik}{}^2 = \|\boldsymbol{v}_k - \boldsymbol{u}_i\|^2, \quad k = 1, 2, \ldots, N_a. \tag{32}$$

$$r_{ik} dr_{ik} = (\boldsymbol{v_k} - \boldsymbol{u_i})^T d\boldsymbol{v}_k, \quad k = 1, 2, \ldots, N_a. \tag{33}$$

$$d\boldsymbol{v}_k = \mathbf{AB} \tag{34}$$

where,

$$\mathbf{A} = \begin{bmatrix} (\boldsymbol{v_k} - \boldsymbol{u_1})^T \\ (\boldsymbol{v_k} - \boldsymbol{u_2})^T \\ \vdots \\ (\boldsymbol{v_k} - \boldsymbol{u_{Na}})^T \end{bmatrix}^{-1}$$

$$\mathbf{B} = \begin{bmatrix} r_{1k} dr_{1k} \\ r_{2k} dr_{2k} \\ \vdots \\ r_{Nak} dr_{Nak} \end{bmatrix}$$

Then the covariance matrix of $\boldsymbol{v}_k$ is

$$\mathbf{D}_{\boldsymbol{v}_k} = \mathbf{A}\mathbf{D}_\mathbf{B}\mathbf{A}^\mathbf{T} \tag{35}$$

where, $\mathbf{D_B}$ is the covariance matrix of B,

$$\mathbf{D_B} = diag\{\sigma_r^2, \sigma_r^2, \ldots, \sigma_r^2\}$$

The random error σ_r^2 are diagonal elements of the covariance matrix $\mathbf{D}_{\boldsymbol{v}_k}$.

For any pair of nodes, we can define the variable equivalent sound speed $\bar{c}$ as the range divided by the traveling time. For any given sound speed profile and node pair, then:

$$r_{ik} = f\,(C\,(z), t_{ik}) = \bar{c}_{ik} t_{ik} \tag{36}$$

here, $\bar{c}$ can be calculated by ray tracing.

In most UWSNs localization scenarios, $1500 m/s$ is assumed to be the sound speed if the compensation for the ray bending is omitted.

$$dr_{ik} = (\bar{c}_{ik} - 1500) t_{ik} = \Delta c_{ik} t_{ik} \le \max_i\{|\Delta c_{ik}|\} t_{ik} \tag{37}$$

Plugging Eq. (37) into Eq. (34)yields the following:

$$\begin{aligned} \varepsilon_c &\leq |\mathbf{A}||\mathbf{B}| \leq |\mathbf{A}|\mathbf{B_1} \\ \mathbf{B_1} &= [r_{1k}t_{1k}, r_{2k}t_{2k}, \ldots, r_{Nak}t_{Nak}]^T \max_{i,j}\{|\Delta c_{ik}|\} \end{aligned} \tag{38}$$

For the systematic error caused by the time delay misalignment, In the k^{th} localization period, we assume that anchor node i and j are the nearest and farthest anchor node to the mobile node respectively, the mobile node locates at position $\boldsymbol{v_{ik}}$ and $\boldsymbol{v_{jk}}$ when the signal from anchor node i and j arrived respectively. Taking the $\boldsymbol{v_{ik}}$ as the reference, the range error dr_{jk} for anchor node j caused by mobility is no greater than the range between $\boldsymbol{v_{ik}}$ and $\boldsymbol{v_{jk}}$, we denote it as Δr_k,

$$dr_{ik} \leq \Delta r_k, \quad i = 1, 2, \ldots, N_a \tag{39}$$

Plugging Eq. (39) into Eq. (34)yields:

$$\begin{aligned} \varepsilon_t &\leq |\mathbf{A}||\mathbf{B}| \leq |\mathbf{A}|\mathbf{B_2} \\ \mathbf{B_2} &= [r_{1k}, r_{2k}, \ldots, r_{Nak}]^T \Delta r_k \end{aligned} \tag{40}$$

We can determine the upper bound of $\boldsymbol{v_k}$ by plugging Eqs. (35), (38) and (40) into Eq. (31).

The best scenario for $\boldsymbol{v_k}$ estimation is one in which there is neither ray bending nor the time delay misalignment, but only random error. In this scenario, the sound speed $C(z)$ can be regarded as a constant C, the localization problem Eq. (4) can be replaced with Eq. (41), and we can determine the lower bound of Eq. (41) by deriving the Cramer-Rao lower bound (CRLB) for $\boldsymbol{v_k}$.

$$\boldsymbol{v}_k = \arg\min_{\boldsymbol{v}_k \in \mathbb{R}^3} \sum_{i=1}^{N_a} (C t_{ik} - \|\boldsymbol{v}_k - \boldsymbol{u}_i\|)^2 \tag{41}$$

V. FIELD TEST EVALUATION

In order to investigate the localization accuracy of the proposed algorithm, we conducted two field experiments: a shallow water experiment and a deep sea experiment. Our method yielded different results between the sets of experiments due to differences in source data and propagation channel quality. We used MATLAB and the CVX toolbox [25] to process the data.

A. SHALLOW WATER EXPERIMENT

The shallow water test was conducted in Qiandao Lake, China, at a depth of about 50 m. Four anchor nodes were laid at the bottom of the lake to form a square with side length of about 400 m. The mobile node to be localized was an AUV. All nodes were synchronized. The anchor nodes were laid about 15 m above the lake bottom and the mobile node was free to move at a depth of 2 m below the water surface. The method established by [26] was used to determine the positions of the anchor nodes in advance. The settings are given in Table 1. The AUV was equipped with an inertial navigation system; the inertial navigation results were used to measure the localization accuracy.

Fig. 4 shows the acoustic velocity profile we measured on-site, which ranged from 1449 m/s to 1507 m/s. After the reception of the localization request issued by the mobile node, the anchor nodes sent localization messages at an interval of 5 s. The mobile node extracted the timestamps after receiving the broadcast messages of the anchor nodes and calculated the bi-directional information interaction propagation time as shown in Fig. 5. The stars labeled 'r-' in Fig. 5 represent the propagation time directly calculated from the timestamp; $a1$ to $a4$ represent the first to fourth anchor nodes, respectively. The points labeled 'f-' represent the propagation time delay output by the proposed method. The proposed method not only eliminated major error points but also output smoother time delays compared to the original time delays, as shown in Fig. 5(b), which is an enlarged view of the rectangular area in Fig. 5 (a).

To display the localization results more clearly, the blue points in Fig. 6 were drawn to represent the difference in propagation time calculated directly from the timestamps while the red points represent the difference in propagation time delay output by the proposed method. The majority of errors arising from small multipath characteristics were eliminated after applying the proposed method.

When there was no acoustic velocity compensation during data processing, the acoustic velocity was set to the empirical value (1500 m/s) and substituted into the formula for computation. Figure 7 shows the localization trajectory of the mobile node in this scenario. The four small black squares in Fig. 7 (a) represent the laid anchor nodes, green points and blue points are the localization results of the JSL method and PCCP algorithm, respectively, and red points are the positions of the final mobile node output by the TA-PCCP with ray tracing. Figure 7 (b) shows an enlarged view of the rectangular area of Fig.7 (a). Table 2 lists the mobile node localization results obtained by various processing methods.

TABLE 1. Coordinates of anchor nodes in the lake experiment (reference to anchor A).

Anchor node	Eastern coordinate (m)	Northern coordinate (m)	Depth (m)
A	0	0	44.95
B	443.06	-315.75	37.66
C	192.67	-726.21	44.87
D	-220.13	-453.91	40.86

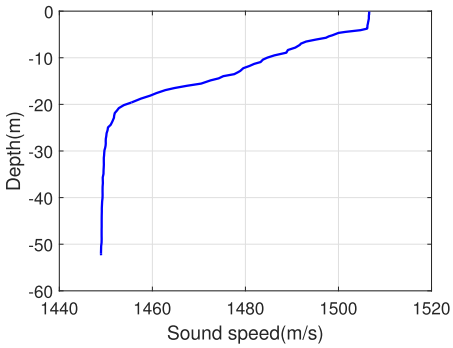

FIGURE 4. The sound velocity profile of the lake experiment.

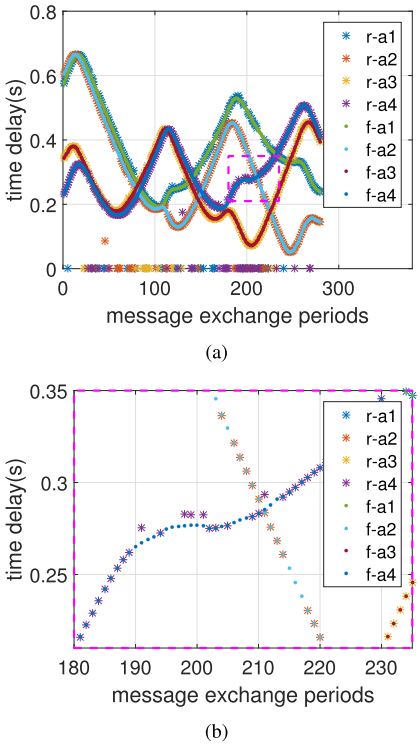

FIGURE 5. Delay calculated from timestamps of the lake experiment ('r': raw data; 'f': final data after processing). (a) Delay. (b) Large view of (a).

As shown in Fig. 7,time alignment effectively eliminated the timestamp measurement errors arising from multipath effects. As shown in Table 2, the localization errors of PCCP decreased from 31.09 m to 10.93 m. The acoustic velocity compensation process decreased the localization errors of PCCP to 29.03 m.The localization results deviate from the actual position in the absence of ray tracing after acoustic velocity compensation in the data processed with TA. After acoustic velocity correction, the final localization RMS error of PCCP decreased to 1.46 m. The Qiandao Lake test site is a small area with a low water depth (50 m) characterized by severe multipath characteristics. To this effect, the acoustic velocity correction did not exert much effect on the data not processed with time alignment. The acoustic velocity correction, however, significantly improved the localization accuracy after time alignment.

As shown in Fig. 7 (a),most of JSL data are consistent with the INS-reference, which indicates that a majority of the coarse data is filtered by IMM filter. However, there are still two serious deviations with the INS-reference in Fig. 7 (a), the detail of one deviations was shown in Fig. 7 (b). And As shown in Fig. 7 and Fig. 5 they are caused by the continuous time-delay estimation error due to the severe multipaths, which leads to the failure of IMM filter. The final RMS error of JSL is 5.17m, which is much bigger than that of TA-PCCP-RT. The experiment in the shallow water shows that TA-PCCP-RT has a better performance than JSL even when the trial data has a poor quality.

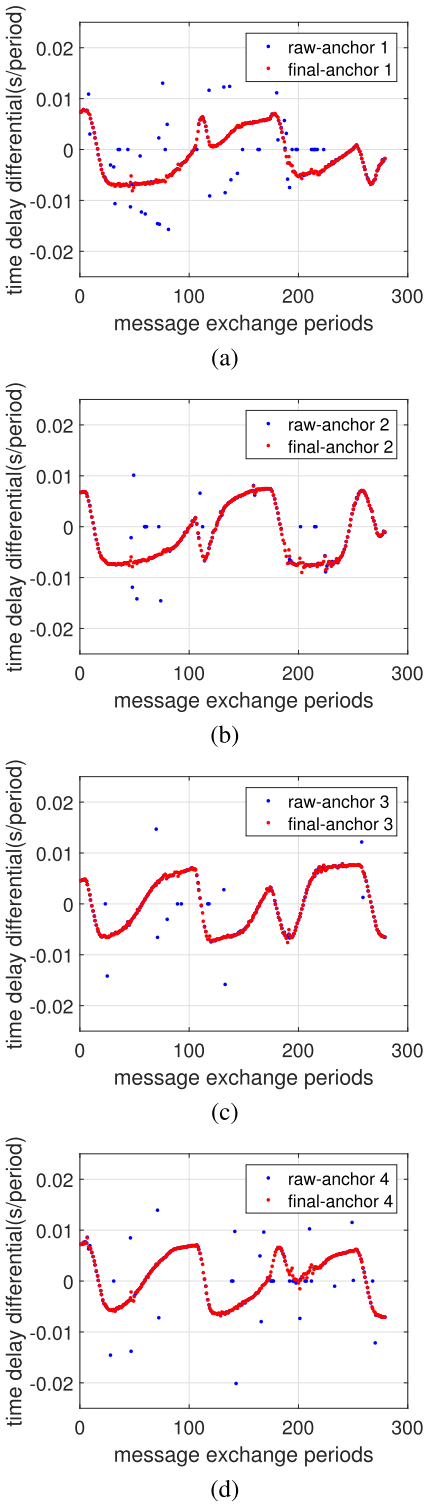

FIGURE 6. Time delay difference of the lake experiment. (a) Anchor 1. (b) Anchor 2. (c) Anchor 3. (d) Anchor 4.

B. DEEP SEA EXPERIMENT

We conducted our deep sea test in the South China Sea at a test area about 3720 m deep. We placed four anchor nodes in a square configuration about 3000 m in length and laid the mobile node at the sea bottom. The anchor nodes were fixed

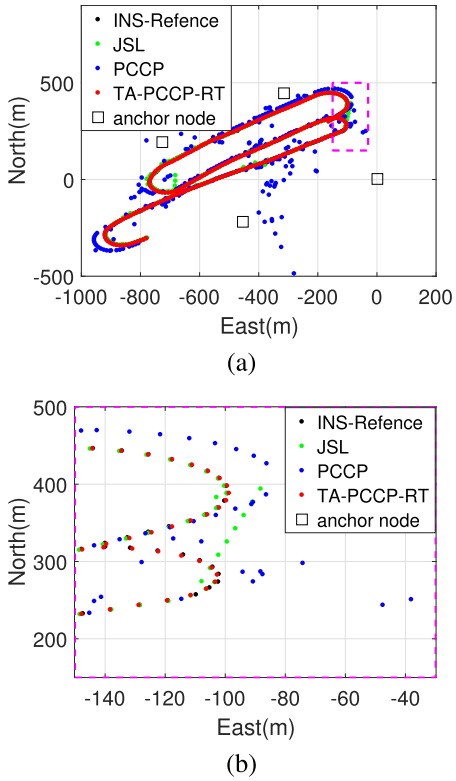

FIGURE 7. Localization results in the lake experiment. (a) Localization results. (b) Large view of (a).

TABLE 2. Localization errors in the lake experiment.

Method	RMS error (m)
JSL	5.17
PCCP	31.09
PCCP-RT	29.03
TA-PCCP	10.93
TA-PCCP-RT	1.46

TABLE 3. Coordinates of anchor nodes in the deep sea experiment (reference to anchor A).

Anchor node	Eastern coordinate (m)	Northern coordinate (m)	Depth (m)
A	0	0	3618.6
B	50.8	-2919.8	3611.6
C	3018.5	-2915.7	3606.7
D	3026.2	36.0	3621.1

about 100 m above the sea bottom. Method in [26] was used to determine the positions of the anchor nodes in advance. The settings are given in Table 3.

The mobile nodes to be positioned were installed in an iron cage which was moved across the back side of the test vessel with a winch, as shown in Fig. 8, with a water entry depth of 10 m. The GPS we used has a wide area differential signal with < 1 m accuracy.

We observed a three-dimensional positional deviation $\boldsymbol{\Delta X}$ from the center of the GPS antenna to the center of the transducer of the mobile nodes to be localized, as shown

FIGURE 8. Installation and laying of the mobile node in the deep sea experiment.

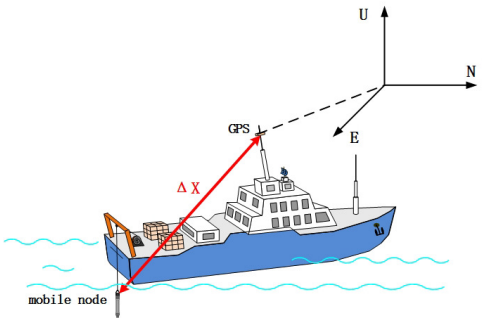

FIGURE 9. Location transformation of the GPS reference in the deep sea experiment.

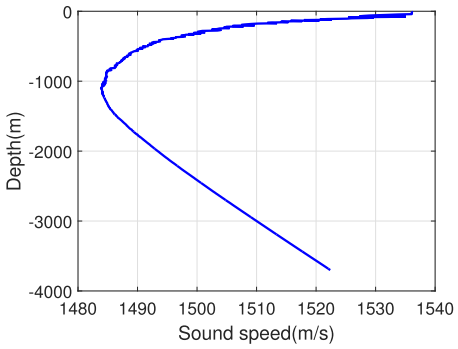

FIGURE 10. The sound velocity profile of the deep sea experiment.

in Fig. 9. By (42), the GPS antenna location of the test vessel $\boldsymbol{X_G}$ was converted into the GPS location information of the transducer of the mobile nodes to be localized $\boldsymbol{X_M}$, as well as the heading/attitude information. The locations of the mobile node as-calculated according to network localization and the GPS position were compared to determine the localization accuracy.

$$\boldsymbol{X_M} = \boldsymbol{X_G} + \boldsymbol{\Psi_{LS}}\boldsymbol{\Delta X}, \tag{42}$$

where $\boldsymbol{\Psi_{LS}}$ is the rotation matrix from the vessel coordinate to the GPS coordinate, given by Eq. (43) shown at the top of the next page.

where $\varphi' = \arcsin(\sin\varphi/\cos\kappa)$, A is the heading of vessel, φ is the pitch of vessel, and κ is the roll of vessel.

Figure 10 shows the acoustic velocity profile measured at the testing site. The sound velocity profile conformed to the typical distribution characteristics of deep-sea acoustic

$$\Psi_{LS} = \begin{bmatrix} \cos\kappa\cos A & \cos\kappa\sin A & \sin\kappa \\ -\cos\varphi'\sin A - \sin\varphi'\sin\kappa\cos A & \cos\varphi'\cos A - \sin\varphi'\sin\kappa\sin A & \sin\varphi'\cos\kappa \\ \sin\varphi'\sin A - \cos\varphi'\sin\kappa\cos A & -\sin\varphi'\cos A - \cos\varphi'\sin\kappa\sin A & \cos\varphi'\cos\kappa \end{bmatrix} \tag{43}$$

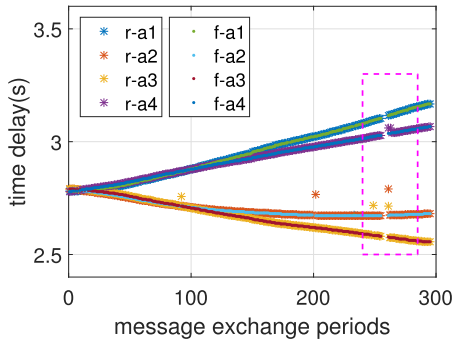

(a)

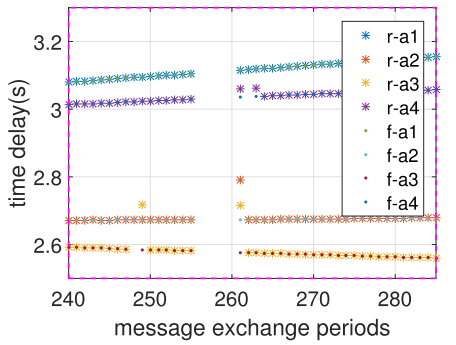

(b)

FIGURE 11. Delay between the mobile node and anchor nodes in the deep sea experiment ('r': raw data; 'f': final data after processing). (a) Delay. (b) Large view of (a).

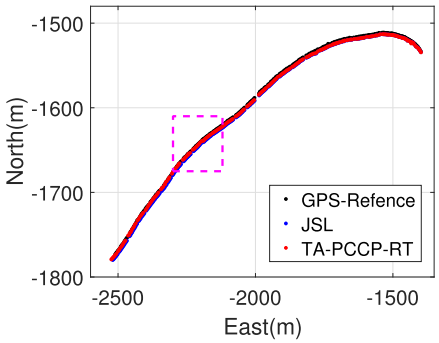

(a)

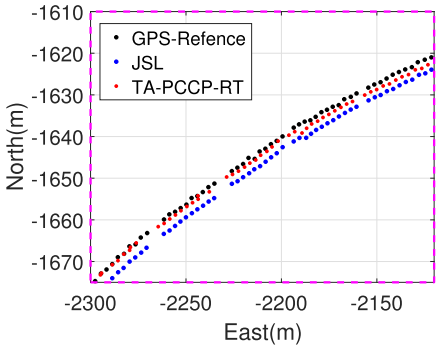

(b)

FIGURE 12. Localization results of the mobile node in the deep sea experiment. (a) Localization results. (b) Large view of (a).

velocity with a sound channel axis located at about 1000 m. The acoustic velocity ranged from 1484 m/s to 1536 m/s.

The anchor node sent localization packets at an interval of 10 s. The mobile node extracted the timestamps after receiving the packets from the anchor nodes and calculated the propagation delays, as shown in Fig. 11. The points in the figure represent the propagation time calculated directly from the timestamp and the curve represents the propagation time delay output by the proposed method. Unlike the lake experiment, the original time delay was of high quality without significant errors arising from multipath interference. There were a few missing points due to communication link failures.

Figure 12 shows the final localization results of the mobile node, where black points represent the location reference gained by GPS, blue points represent the location of the mobile node calculated by JSL, and red points represent the location of the mobile node calculated by PCCP with time alignment and sound velocity compensation. As shown in Fig. 12(a), both stes of localization results are close to the reference. Fig. 12(b) shows an enlarged image of the rectangular area in Fig. 12(a), where the TA-PCCP-RT results are much closer to the GPS reference than the JSL results.

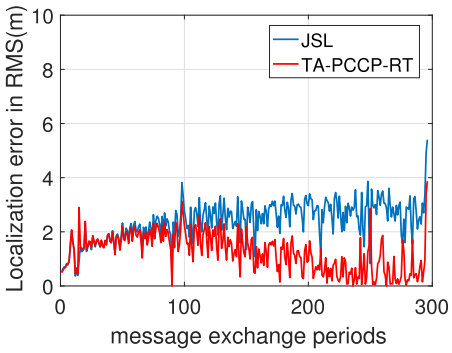

FIGURE 13. Localization error comparison between JSL and PCCP in the deep sea experiment.

Fig. 13 and Table 4 shows the final RMS errors obtained via different processing methods. The errors arising from acoustic velocity were significantly greater than those from unaligned timestamps in the absence of acoustic velocity correction. The anchor nodes were laid at the sea bottom while the mobile nodes were operated near the sea surface, as described above; the depth between the mobile and anchor

TABLE 4. Localization errors of various processing methods in deep sea experiment.

Method	RMS error (m)
JSL	2.98
PCCP	37.73
PCCP-RT	2.38
TA-PCCP	37.81
TA-PCCP-RT	1.44

nodes spanned about 3600 m, so acoustic velocity errors were a major source of error. In addition, the raw time delay were of high quality, so timestamp alignment did not significantly affect the localization accuracy. Sound ray tracing reduced the localization error of PCCP from 37.73 m to 2.38 m.

As shown in Table 4, the localization error for JSL and TA-PCCP-RT are 2.98 m and 1.44 m respectively, the TA-PCCP-RT shows a significant improvement in accuracy. Unlike the shallow water experiment results, JSL did not deviate from the INS-reference in the deep water experiment as there were few outliers in the time-delay estimation.

VI. CONCLUSION

Localization for mobile nodes is a challenging issue inherent to UWSNs. Range errors lead to significant localization errors due to fluctuations in sound transmission speed. Errors originate in two main sources: different locations of the mobile node as it receives timestamps from different anchor nodes in the same localization period, and ray bending. This paper presented a new mobile node localization framework which includes Kalman filter based time alignment, sound ray tracing, and nonconvex optimization tools. The proposed method includes aligning the timestamps from various neighboring anchor nodes via a Kalman filter followed by a special initialization; a feedback controller then rapidly initiates the Kalman filter and inhibits divergence. Sound ray tracing has been used to determine the accurate distance between the neighboring anchor nodes and the mobile nodes, and to shorten the propagation time between nodes based on distance.

We solved the nonconvex optimization network localization problem using PCCP, and found that the combination of time alignment and sound ray tracing yields favorable PCCP solutions. Shallow water experiments revealed that TAPCCP-RT outperforms JSL in the case of severe multipath. Deep sea experimental results (3700 m depth, with differential GPS as true-value reference) showed final TA-PCCP-RT localization errors of 1.44 m only and JSL results of 2.98 m,; in other words, the localization errors of TA-PCCP-RT are 48.3% of that of JSL.

REFERENCES

[1] J. Heidemann, W. Ye, J. Wills, A. Syed, and Y. Li, "Research challenges and applications for underwater sensor networking," in *Proc. IEEE Wireless Commun. Netw. Conf. (WCNC)*, vol. 1, Apr. 2006, pp. 228–235.

[2] J. Heidemann, M. Stojanovic, and M. Zorzi, "Underwater sensor networks: Applications, advances and challenges," *Philos. Trans. Roy. Soc. London A, Math. Phys. Sci.*, vol. 370, no. 1958, pp. 158–175, Jan. 2012.

[3] H.-P. Tan, R. Diamant, W. K. G. Seah, and M. Waldmeyer, "A survey of techniques and challenges in underwater localization," *Ocean Eng.*, vol. 38, nos. 14–15, pp. 1663–1676, Oct. 2011.

[4] V. Chandrasekhar, W. K. Seah, Y. S. Choo, and H. V. Ee, "Localization in underwater sensor networks: Survey and challenges," in *Proc. 1st ACM Int. Workshop Underwater Netw.*, 2006, pp. 33–40.

[5] M. Erol-Kantarci, H. T. Mouftah, and S. Oktug, "A survey of architectures and localization techniques for underwater acoustic sensor networks," *IEEE Commun. Surv. Tuts.*, vol. 13, no. 3, pp. 487–502, Mar. 2011.

[6] R. J. Urick, *Principles of Underwater Sound for Engineers*. New York, NY, USA: McGraw-Hill, 1967.

[7] Y. Han, Y. R. Zheng, and D. Sun, "Measurement error impact on node localization of large scale underwater sensor networks," in *Proc. IEEE 82nd Veh. Technol. Conf. (VTC Fall)*, Sep. 2015, pp. 1–5.

[8] R. Diamant and L. Lampe, "Underwater localization with time-synchronization and propagation speed uncertainties," *IEEE Trans. Mobile Comput.*, vol. 12, no. 7, pp. 1257–1269, Jul. 2013.

[9] J. Yi, D. Mirza, C. Schurgers, and R. Kastner, "Joint time synchronization and tracking for mobile underwater systems," in *Proc. 8th ACM Int. Conf. Underwater Netw. Syst.*, 2013, Art. no. 38.

[10] J. Yi, D. Mirza, R. Kastner, C. Schurgers, P. Roberts, and J. Jaffe, "TOA-TS: Time of arrival based joint time synchronization and tracking for mobile underwater systems," *Ad Hoc Netw.*, vol. 34, pp. 211–223, 2015.

[11] J. Liu, Z. Wang, J.-H. Cui, S. Zhou, and B. Yang, "A joint time synchronization and localization design for mobile underwater sensor networks," *IEEE Trans. Mobile Comput.*, vol. 15, no. 3, pp. 530–543, Mar. 2016.

[12] Z. Paul and M. Howard, *Fundamentals of Kalman Filtering: A Practical Approach*. Reston, VA, USA: AIAA, 2005.

[13] J. Zhang, D. Sun, and C. Ji, "A LBL positioning method based on feedback Kalman filter," *Sensors Transducers*, vol. 163, no. 1, pp. 161–165, 2014.

[14] G. Ji-jie, "Measurement data of underwater acoustic positioning in location of a tow-body and Kalman filter," in *Proc. Chin. Conf. Underwater Acoust.*, 2001, pp. P7–P11.

[15] L. Minzan, "Post processing technology of underwater acoustic accurate position," M.S. thesis, College Underwater Acoust. Eng., Harbin Eng. Univ., Harbin, China, 2008.

[16] P. Carroll, K. Mahmood, S. Zhou, H. Zhou, X. Xu, and J.-H. Cui, "On-demand asynchronous localization for underwater sensor networks," *IEEE Trans. Signal Process.*, vol. 62, no. 13, pp. 3337–3348, Jul. 2014.

[17] H. Kulhandjian and T. Melodia, "A low-cost distributed networked localization and time synchronization framework for underwater acoustic testbeds," in *Proc. IEEE Underwater Commun. Netw. (UComms)*, Sep. 2014, pp. 1–5.

[18] K. W. Cheung, W. K. Ma, and H. C. So, "Accurate approximation algorithm for toa-based maximum likelihood mobile location using semidefinite programming," in *Proc. IEEE Int. Conf. Acoust., Speech, Signal Process. (ICASSP)*, vol. 2. May 2004, pp. II-145–II-148.

[19] A. Beck, P. Stoica, and J. Li, "Exact and approximate solutions of source localization problems," *IEEE Trans. Signal Process.*, vol. 56, no. 5, pp. 1770–1778, May 2008.

[20] I. Darya and L. Wu-Sheng, "Penalty convex-concave procedure for source localization problem," in *Proc. IEEE Can. Conf. Elect. Comput. Eng. (CCECE)*, May 2016, pp. 1–4.

[21] T. Lipp and S. Boyd, "Variations and extension of the convex–concave procedure," *Optim. Eng.*, vol. 17, no. 2, pp. 263–287, 2014.

[22] R. Diamant, H.-P. Tan, and L. Lampe, "LOS and NLOS classification for underwater acoustic localization," *IEEE Trans. Mobile Comput.*, vol. 13, no. 2, pp. 311–323, Feb. 2014.

[23] M. Stojanovic, "Underwater acoustic communications," in *Proc. IEEE Electro/95 Int. Prof. Program*, Jun. 1995, pp. 435–440.

[24] M. R. Allen and L. A. King, "An adaptive two stage Kalman structure for passive undersea tracking," *IEEE Trans. Acoust., Speech Signal Process.*, vol. 36, no. 1, pp. 3–9, Jan. 1988.

[25] I. CVX Research. (Aug. 2012). *CVX: MATLAB Software for Disciplined Convex Programming, Version 2.0*. [Online]. Available: http://cvxr.com/cvx

[26] F. N. Spiess, C. D. Chadwell, J. A. Hildebrand, L. E. Young, G. H. Purcell, Jr., and H. Dragert, "Precise gps/acoustic positioning of seafloor reference points for tectonic studies," *Phys. Earth Planetary Interiors*, vol. 108, no. 2, pp. 101–112, 1998.

CUIE ZHENG (M'14) received the B.Sc. and Ph.D. degrees in underwater acoustic engineering from Harbin Engineering University, Harbin, China, in 2004 and 2008, respectively. Since 2006, she has been with the College of Underwater Acoustic Engineering, Harbin Engineering University, where she is currently an Associate Professor. She was with the University of Victoria as a Visiting Scholar from 2016 to 2017. Her research interests lie in the algorithms and applications of underwater acoustic localization and navigation.

DAJUN SUN (M'15) received the B.Sc., M.Sc., and Ph.D. degrees in underwater acoustic engineering from Harbin Engineering University, Harbin, China, in 1994, 1996, and 1999, respectively. He has been with Harbin Engineering University since 1996. From 2001 to 2002, he was a Visiting Scholar with the National University of Singapore. He became a Professor in 2007. His research focuses on sonar system design and application research, including long/short-baseline localization sonar, Dopper velocity logs, communication sonar, submerged buoy systems, and imaging sonar.

LIN CAI (S'00–M'06–SM'10) received the M.A.Sc. and Ph.D. degrees in electrical and computer engineering from the University of Waterloo, Waterloo, ON, Canada, in 2002 and 2005, respectively. Since 2005, she has been with the Department of Electrical and Computer Engineering, University of Victoria, where she is currently a Professor. Her research interests span several areas in communications and networking, with a focus on network protocol and architecture design supporting emerging multimedia traffic over wireless, mobile, ad hoc, and sensor networks. She was a recipient of the NSERC Discovery Accelerator Supplement Grants in 2010 and 2015, respectively, and the Best Paper Awards of the IEEE ICC 2008 and the IEEE WCNC 2011. She served as a TPC Symposium Co-Chair for the IEEE GLOBECOM'10 and GLOBECOM'13. She served as a Distinguished Lecturer for the IEEE VTS Society. She served as an Associate Editor for the IEEE TRANSACTIONS ON WIRELESS COMMUNICATIONS, the IEEE TRANSACTIONS ON VEHICULAR TECHNOLOGY, the *EURASIP Journal on Wireless Communications and Networking*, the *International Journal of Sensor Networks*, and the *Journal of Communications and Networks*.

XIANG LI received the B.Sc., M.Sc., and Ph.D. degrees in underwater acoustic engineering from Harbin Engineering University, Harbin, China, in 2002, 2005, and 2011, respectively. He has been with Harbin Engineering University since 2005. His research focuses on underwater positioning and navigation, including long/short-baseline localization sonar and Dopper velocity logs.